Global X-ray emission during an isolated substorm - A case study

N. Østgaard,[1] J. Stadsnes,[1] and J. Bjordal[1]
R. R. Vondrak[2] and S. A. Cummer[2]
D. L. Chenette[3] and M. Schulz[3]
G. K. Parks[4] and M. J. Brittnacher[4]
D. L. McKenzie[5]
J. G. Pronko[6]

Abstract. The Polar Ionospheric X-ray Imaging Experiment (PIXIE) and the UV imager (UVI) onboard the Polar satellite have provided the first simultaneous global scale views of the patterns of electron precipitation through imaging of the atmospheric X-ray bremsstrahlung and the auroral UV emissions. While the UV images in the Lyman-Birge-Hopfield-long (LBHL) band used in this study respond to the total electron energy flux which is usually dominated by low-energy electrons (<10 keV), the PIXIE images of X-ray bremsstrahlung above 2.7 keV respond to electrons of energy above ~3 keV. Comparison of precipitation features seen by UVI and PIXIE provides information on essentially complementary energy ranges of the precipitating electrons. In this study an isolated substorm is examined using data from PIXIE, UVI, ground-based measurements, and in situ measurements from high- and low-altitude satellites to obtain information about the global characteristics during the event. Results from a statistical study of isolated substorms, which has reported a significant difference in the patterns of energetic electron precipitation compared to the less energetic precipitation are confirmed. A localized maximum of electron precipitation in the morning sector delayed with respect to substorm onset is clearly seen in the X-ray aurora, and the time delay of this morning precipitation relative to substorm onset strongly indicates that this intensification is caused by electrons injected in the midnight sector drifting into a region in the dawnside magnetosphere where some mechanism effectively scatter the electrons into the loss cone. In this study we also present the results from two low-altitude satellite passes through the region of the localized maximum of X-ray emission in the morning sector. Measured X rays are compared with X-ray fluxes calculated from the electron spectral measurements. By fitting the electron spectra by a sum of two exponentials we obtain fairly good agreement between calculated and directly measured X-ray flux profiles.

1. Introduction

The International Solar Terrestrial Physics (ISTP) program provides a unique opportunity to study the global substorm. Combining satellite monitoring, ground-based measurements, and remote sensing techniques such as visible, ultraviolet (UV) and X-ray imaging one might be able to establish a comprehensive picture of the substorm development in the entire energy range of precipitating electrons taking part in the global substorm [Robinson and Vondrak, 1994]. The first global schematics of the auroral substorm were based on statistical studies of data from a large number of all-sky camera stations [Akasofu, 1964; Akasofu, 1968; Feldstein and Starkov, 1967]. Many of the large-scale features from these schematics have been confirmed by global UV imagers and visible imagers. As UV and visible emissions are proportional to the total electron energy flux which is usually dominated by electron energies below 10 keV, the global UV and visible images mainly display the patterns of the low-energy electron precipitation. Visible imagers are also restricted to image only the night side aurora due to contamination by sunlight.

Until recently global imaging of the energetic electron precipitation has not been available. Our knowledge of how the precipitating energetic electrons behave during substorms has been based on measurements of cosmic radio noise absorption (riometer) [Hartz and Brice, 1967; Jelly and Brice, 1967; Berkey et al., 1974], X-ray measurements from balloon campaigns [Bjordal et al., 1971; Sletten et al., 1971; Kangas et al., 1975], particle measurements in space [McDiarmid et al., 1975; Hardy et al., 1985] and X-ray measurements from low-altitude satellites [Imhof et al., 1980; Chenette et al., 1992]. The Polar Ionospheric X-ray Imaging Experiment (PIXIE) [Imhof et al., 1995] onboard the Polar satellite is the first true two-dimensional imaging instrument developed to measure the global X-ray emission simultaneously. As the X rays are produced by high-energy electrons interacting with the contents of the ionosphere, PIXIE provides the ability of studying both the spatial and temporal patterns of the global energetic electron precipitation during substorms.

From several statistical studies based on satellite measurements [McDiarmid et al., 1975; Hardy et al., 1985], riometer measurements [Hartz and Brice, 1967; Jelly and Brice, 1967; Berkey et al., 1974] and global images in UV [Liou et al., 1997] and X rays [Petrinec et al., 1998] there are found to exist two maximum regions of energetic precipitation but three maxima in the softer precipitation (<1 keV). McDiarmid et al. [1975] and Hardy et al. [1985] studied electron measurements in the energy range from tens of eV up to tens of keV, while Jelly and Brice [1967] and Berkey et al. [1974] studied absorption of cosmic radio noise, which is sensitive to electrons of energies from 10 to 100 keV. Focusing on the energetic precipitation all these studies found the first and most intense maximum to be situated around midnight and to be related to the injection of fresh electrons. They found another maximum to be located between dawn and noon, most probably related to the drifting electrons. However, by focusing on electron

---
[1]Department of Physics, University of Bergen, Bergen, Norway.
[2]Laboratory for Extraterrestrial Physics, Goddard Space Flight Center, Greenbelt, Maryland.
[3]Lockheed-Martin Advanced Technology Center, Palo Alto, California.
[4]Geophysics Program, University of Washington, Seattle.
[5]The Aerospace Corporation, Los Angeles, California.
[6]Physics Department, University of Nevada, Reno, Nevada.

precipitation at lower energies (<1 keV) there is found to exist an additional maximum in the postnoon region [McDiarmid et al., 1975; Liou et al., 1997] where an almost complete lack of X-ray emission is observed [Petrinec et al., 1998]. All of these studies, except for the study of Berkey et al. [1974], were based on adding all the observed precipitation during all kind of geomagnetic activity, and provide no information on the temporal behaviour of single substorms. However, a statistical study of 14 isolated substorms during 1996 [Østgaard et al., 1999b] using PIXIE and UVI data from the Polar satellite combined with ground-based measurements and data from geosynchronous satellites have confirmed many of these global characteristics.

To further investigate the global features of both soft and energetic precipitation during isolated substorms we will present an isolated substorm from 1997 where both the low-energy and high-energy range X rays were detected by PIXIE. Particle measurements obtained in the injection region in the magnetotail and at geosynchronous orbit are examined. Electron measurements from low-altitude satellite passes through the region of the localized maximum in the morning sector are used to compare calculated X rays from electron spectra with the directly measured X rays.

2. Observations and Interpretation

To examine the temporal behaviour of the energetic electron precipitation during substorms and particularly the localized maximum seen in the morning sector delayed relative to the substorm onset, we have looked for an isolated substorm when PIXIE was detecting both the low-energy X rays (~3 keV-10 keV) and the high-energy range (~10-20 keV). Due to a problem with the high-voltage supply in the front chamber of the PIXIE instrument, which measures the low-energy X rays, the front chamber had to be duty cycled with 5 min on and 10 min off for most of 1997. However, the rear chamber measuring the high-energy X rays provides continuous measurements. The substorm occurring at ~1108 UT September 4, 1997 complied with these constraints. In Figure 1 the magnetic conditions during the substorm are shown. From the AE index the isolated nature of this event is clearly seen. The AE index rises from quiet conditions up to 650 nT and recovers to about 0 nT during this substorm. Data from all the 8 stations in the Kyoto data base are included to obtain the AE index. We see from the Dst index in of Figure 1a that the substorm occurred in the recovery phase of a substantial magnetic storm which reached a minimum of -150 nT the day before. However, the Kp index was only 2 at the time the substorm occurred.

In Figure 2 the locations of the various spacecrafts providing data for this study are shown. From Figure 2a we see that the Polar satellite, providing X-ray data from PIXIE [Imhof et al., 1995] and UV data from the ultraviolet imager (UVI) [Torr et al., 1995] was in an apogee pass, well situated to image the global aurora in the northern hemisphere. From Figure 2b an equatorial view shows that Geotail was located close to midnight in the magnetic tail at 10 R_E well situated to observe the injection of particles at the onset of the substorm. The geosynchronous Los Alamos spacecraft, SC 1994-084 was located in the evening sector at ~18 magnetic local time (MLT).

In Plate 1 the UV images and the PIXIE images are shown. Left panels show the UV images in the Lyman-Birge-Hopfield-long (LBHL) band having a 37 seconds exposure time. This band is dominated by the emission created by the electron impact on N_2. All electron energies contribute in this process, and as the absorption of LBHL emissions by atmospheric oxygen is negligi-
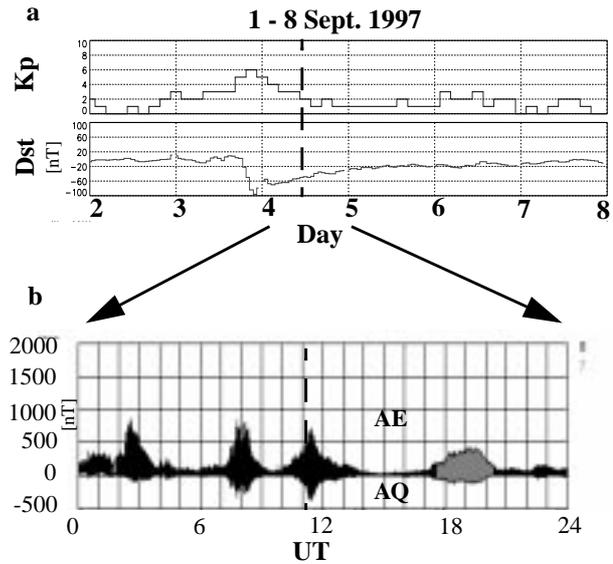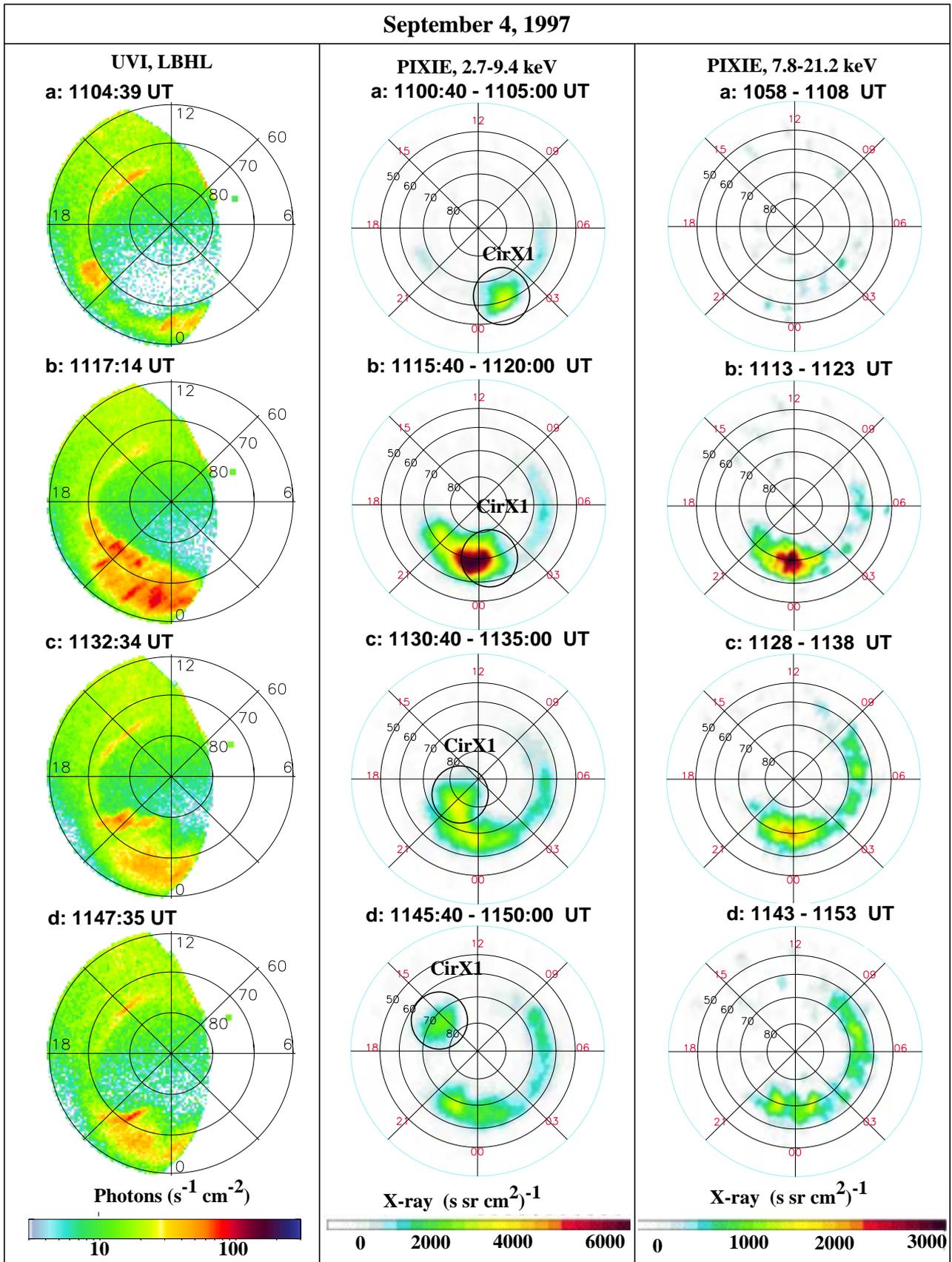

Figure 1. (a) Dst and Kp indices during the event. (b) Provisional AE index from Kyoto, based on all the 8 stations. The dashed line indicates the onset time of the substorm.
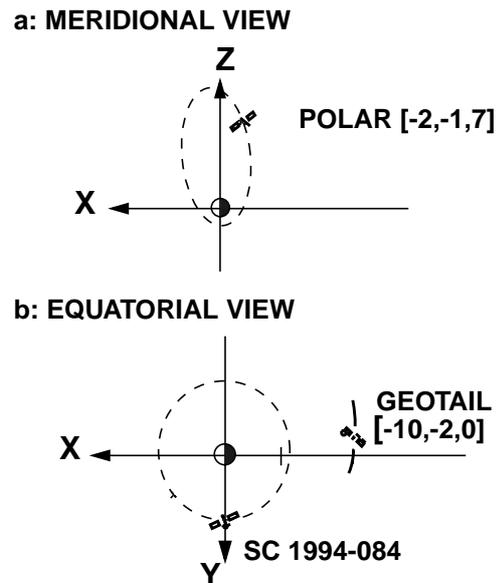

Figure 2. Meridional and equatorial view of the spacecraft locations at 1108 UT September 4, 1997

ble (below ~10 keV), the intensity reflects the total energy influx of electron precipitation. The electron energies, which UVI is sensitive to, are estimated to be from 1 keV to 10 keV given an energy flux of 1 erg (cm² s)⁻¹. For larger energy fluxes the threshold may be lowered down to about 100 eV (G. Germany private communication, 1998). Middle panel shows 5 min accumulation of PIXIE images in the energy range 2.7-9.4 keV. These X rays are produced by electron energies above ~3 keV. Right panel shows 10 min accumulation of PIXIE images in the energy range 7.8-21.2 keV, which are produced by electron energies above ~8 keV. Both panels of X-ray images have approximately the same center time,

September 4, 1997

UVI, LBHL	PIXIE, 2.7-9.4 keV	PIXIE, 7.8-21.2 keV
a: 1104:39 UT	a: 1100:40 - 1105:00 UT	a: 1058 - 1108 UT
b: 1117:14 UT	b: 1115:40 - 1120:00 UT	b: 1113 - 1123 UT
c: 1132:34 UT	c: 1130:40 - 1135:00 UT	c: 1128 - 1138 UT
d: 1147:35 UT	d: 1145:40 - 1150:00 UT	d: 1143 - 1153 UT

Photons (s^{-1} cm^{-2})

X-ray (s sr cm^2)$^{-1}$

X-ray (s sr cm^2)$^{-1}$

Plate 1. (left) UV images in the Lyman-Birge-Hopfield-long (LBHL) band, exposure time 37 seconds. (middle) Integral X-ray flux in the energy range from 2.7 keV to 9.4 keV, 5 min accumulation. The celestial source Circinus X-1 is encircled. (right) Integral X-ray flux in the energy range from 7.8 keV to 21.2 keV, 10 min accumulation. Corrected geomagnetic (CGM) grid is used in all the panels.
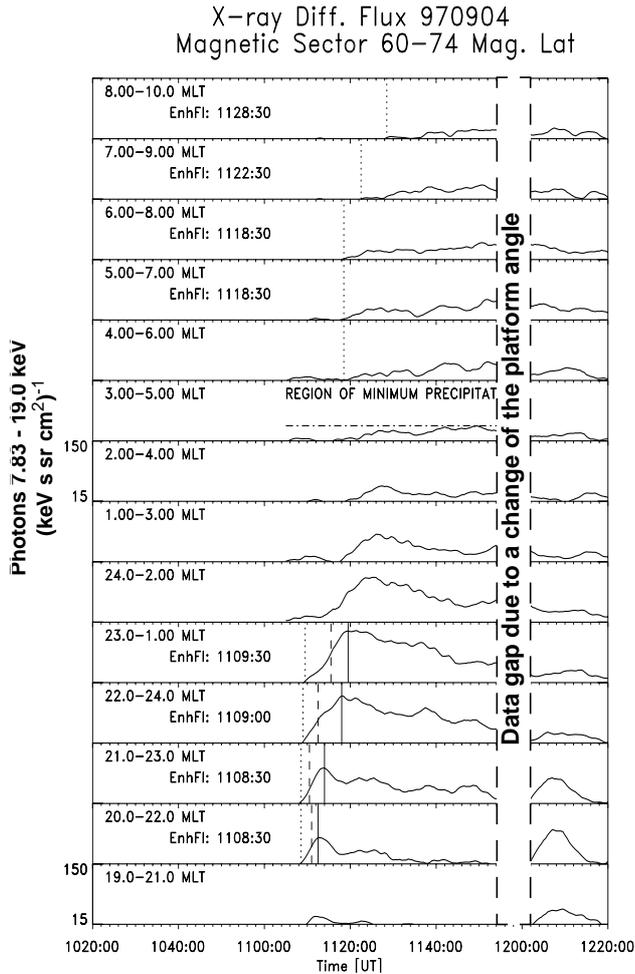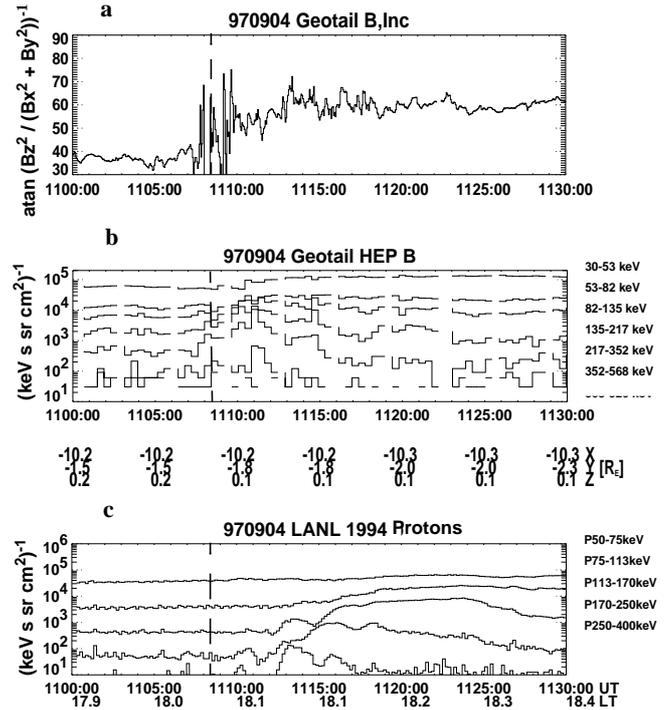
Figure 3. Time development of the mean differential X-ray fluxes in sectors from 19-21 to 8-10 MLT and fixed magnetic latitude 60°-74°. Dotted lines indicate the onset of X-ray emission.

Figure 4. Measurements by Geotail situated at [-10,-2,0] GSM and LANL SC 1994-084 in geostationary orbit. (a) Inclination of magnetic field lines measured by Geotail. (b) Ion measurements from HEP at Geotail. (c) Proton measurements by LANL SC 1994-084. The dashed line indicates the onset time at 1108 UT identified from the X-ray measurements.

but are accumulated differently in order to obtain sufficient statistics to process images. Further information about the image processing can be found in [Østgaard et al., 1999a].

In all the low-energy X-ray images in the middle panel the celestial source Circinus X-1 is seen, entering at slant angle through adjacent pinholes of the PIXIE camera. Circinus X-1 is moving across the image as the Polar satellite proceeds in its orbit. As the energy spectrum of this neutron-star binary X-ray source is rather soft, it is not detectable in the higher energy range of X rays shown in the right panel.

From the UV images Plate 1a (left) we see soft electron precipitation prior to the substorm onset in the postnoon sector which is totally absent in the X-ray images (middle and right). In the UVI we also see a localized bright region around 20 MLT which appeared about 1100 UT (images not shown). As this bright region does not expand or increase in intensity for at least the next 5 min, we think this is another growth phase signature which corresponds well with the AE index around that time. This bright region is just barely seen in the low-energy X-ray image in Plate 1a (middle) indicating relatively soft electron precipitation. From images not shown the UV substorm onset is determined to occur between 1105 UT and 1108 UT at about 21 MLT (no images were available between 1105 UT and 1108 UT) expanding

both westward and eastward with time. In Plate 1b the westward edge has moved about one hour local time duskward in ~12 min giving an average westward travelling surge (WTS) velocity of about 0.8 km/s. From the X-ray images (middle and right panels) we see the precipitation region expands eastward and in Plate 1d we see the localized morning maximum appears in both of the energy ranges of X rays. Unfortunately, due to the smaller field of view (FOV) of the UVI, we have no UV measurements in the morning sector during this event and we are not able to tell if this feature involves low electron energies as well. However, from several statistical studies [Jelly and Brice, 1967; Berkey et al., 1974; McDiarmid et al., 1975; Hardy et al., 1985] it is believed that this localized maximum of precipitation involves mainly energetic electrons. From the statistical study of Østgaard et al. [1999b] it was reported that this morning maximum was rarely seen by the UVI but was a common feature in the PIXIE images, which indicated precipitation of rather energetic electrons.

In Figure 3 the time development of the high-energy X-ray emission (7.8-19.0 keV) in the 2 hour MLT sectors from 19 to 10 MLT is shown. These X-ray measurements are continuous and not contaminated by the Circinus X-1. In the north-south direction all sectors extend from 60° to 74° corrected geomagnetic (CGM) latitude. 5 min accumulations of X rays sampled every 30 s and a running average of 3 (i.e., 1.5 min) are used. The end of the accumulation time interval is used at the abscissa, giving about a 1 min resolution for the timing of onset, but about 2.5 min too late timing of the maxima (as the center time should be used for the

maxima). To improve the statistics 2 hour MLT sectors were chosen. For fluxes of 100 (keV s sr cm2)$^{-1}$ the σ is about 30%. The data gap between 1155 and 1203 UT is due a change in the platform angle, which smears out the X-ray images in this time interval. The X-ray substorm onset is found to occur in the 21-22 MLT sector at 1108:30 UT, which corresponds fairly well with the onset time determined from the UVI taking into account the 1 min time resolution of the X-ray measurements and the 37 s exposure time from the UVI. The X-ray features are expanding eastward into the morning sector. In the sectors from 4 to 9 MLT the localized maximum in the morning sector can be seen. The onset of the localized maximum can be identified from the 5-7 MLT sector to be 1118.30 UT, but could be identified from the adjacent sectors as well. Although there is a weak enhancement of X-ray emission in the 19-21 MLT sector 1 min later than the substorm onset in the 21 MLT sector it can hardly be interpreted as any westward expansion (WTS) of the X-ray features.

A movie of the entire X-ray substorm in the energy range of 7.8-21.2 keV can be found at the URL address: http://www.fi.uib.no/~nikolai/PIXIE-mov/970904.html. The movie clearly shows the eastward expansion and the localized morning maximum of X-ray emission.

In Figure 4 the magnetic field and particle measurements from Geotail are shown along with the proton measurements from the Los Alamos National Laboratory (LANL) SC 1994-084. From Figure 4b an injection of protons is seen most significantly in the 217-352 keV channel coincidentally with the signatures of the dipolarization of the field lines (Figure 4a) about one minute before the onset of the X-ray substorm, which is about the uncertainty of the onset time determined from the PIXIE measurements (Figure 3) and in very good agreement with the UV substorm onset time. These measurements from Geotail strongly indicate that the current wedge is formed very close to 10 R_E. The SC 1994-084 observes the injection some minutes later as should be expected due to the gradient and curvature drift of protons injected 2-3 MLT sectors east of the spacecraft.

From Figure 3 we identified the substorm onset time to be at 1108:30 UT (21-22 MLT sector) and the onset of the localized maximum in the morning sector at 1118:30 UT (5-7 MLT sector). The time delays of 10.5 min are plotted in Figure 5 along with the time delays along the auroral zone for 7 other isolated substorms from 1996 and 1997. Assuming the X-ray features to be caused by electrons injected at midnight and drifting eastward into the morning sector the time delays between the substorm onset and the appearance of X-ray emissions at different local times along the auroral zone, can be used to calculate the electron energies that correspond to the observed time delays. Both a simple dipole drift model [Lew, 1961] and a more realistic model which takes the azimuthal assymmerty of the field lines into account [Roederer, 1970] can be used for this purpose. From the statistical study of Østgaard et al. [1999b] it was shown that the model of Roederer [1970] tended to give 5-20 keV lower energies than the model of Lew [1961], but for most of the substorms this discrepancy was smaller than the uncertainties of the determination of time delays. Keeping this in mind the model of Lew [1961] can be used to plot the time delays for drifting electrons of different energies in the same plot as the observed time delays of X-ray features. Figure 5 shows that for 8 substorms from 1996 and 1997 the time delays of X-ray features along the auroral zone correspond to precipitation from drifting electrons in the energy range of 90-170 keV. These findings confirm the results from Sletten et al. [1971], ~140 keV, Kangas et al. [1975], 100-200 keV, and Berkey et al.
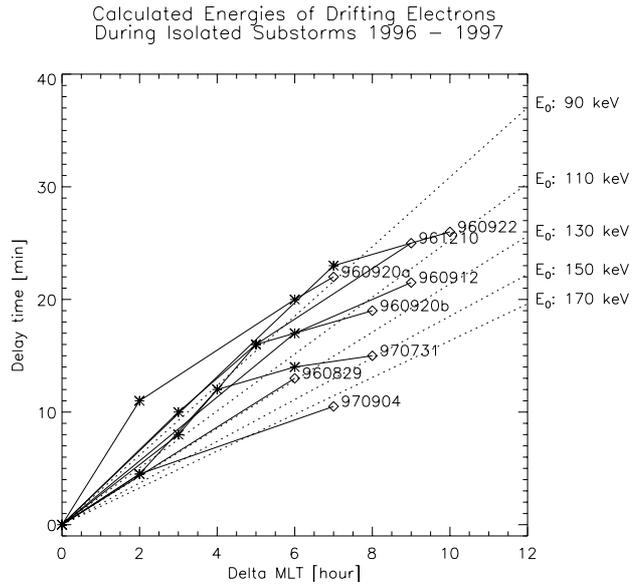
Figure 5. Delay time from substorm onset to the onset of the X-ray emission at different local time sectors along the auroral zone Dotted lines show delay time versus MLT sectors for energies from 90 keV to 170 keV using the drift model of Lew [1961].

[1974], 100 keV. Notice that these high energies correspond to the first-arriving electrons which produce the first enhancement of X rays along the auroral zone and that electrons at lower energies probably account for the subsequent increase of the observed X rays. In 7 of the 8 cases shown in Figure 5 we observe an apparent increase of electron energies when the X-ray features arrive the morning sector (i.e., at high Delta MLT values). The uncertainties of time delay determination is ~1 min but as this tendency is seen in 7 of 8 cases the apparent energy increase seems to be significant. If the model of Roederer [1970] was used instead of Lew [1961] the dotted lines indicating energies in Figure 5 would not have been linear but would have a steadily increasing slope as the drift velocity decreases towards the dayside. Thus, this implies an even stronger energy increase than shown in Figure 5. This apparent energy increase of ~10-30 keV may be associated with an electric potential drop along the drift path. To give the observed electron energy increase the electric field must have a westward component along the drift path with a maximum in the morning sector, which is not very likely. However, we do not think there is any additional energization in the morning sector but that the trend observed must rather be explained by a wave-particle interaction which is more favourable for these high energy electrons in the 5-9 MLT region than in the earlier local time sectors. This explanation requires that the electron cloud becomes rather anisotropic when entering the morning sector. This has been modelled by Jentsch [1976] and observed by Isenberg et al. [1982]. As the electrons reach the morning sector where the conditions for wave growth [Parrot and Gaye ,1994] and electron scattering [Isenberg et al., 1982] are very good the fluxes of high energy precipitating electrons may increase due to pitch angle diffusion and give these signatures of apparent energy increase.

In Figure 6 and Figure 7 we have examined the electron precipitation within the loss cone measured by low-altitude satellites for two different passes through the region of the localized maximum of X-ray emission in the morning sector. National Oceanic
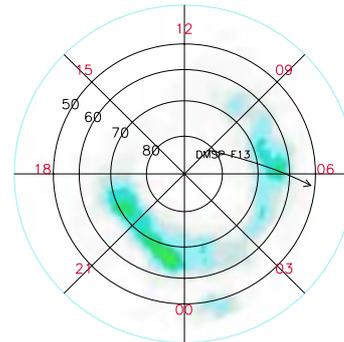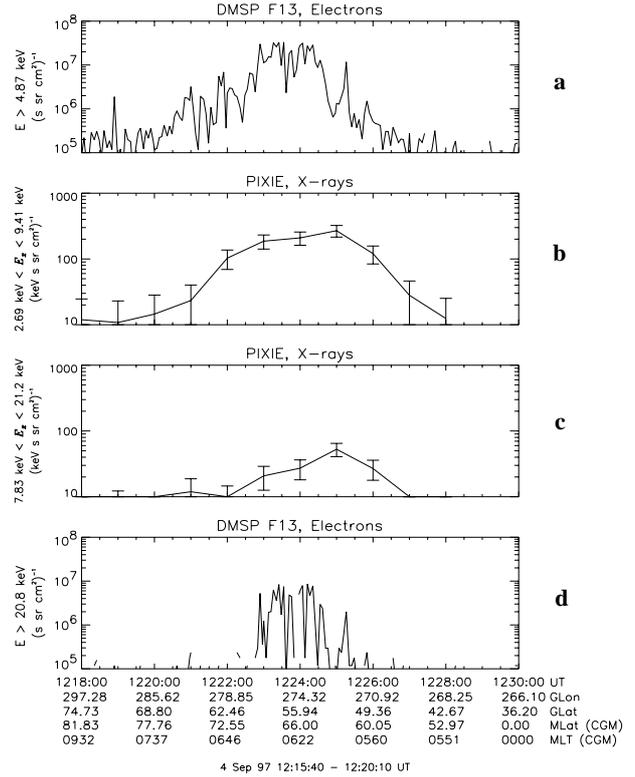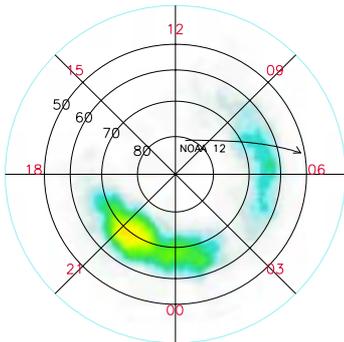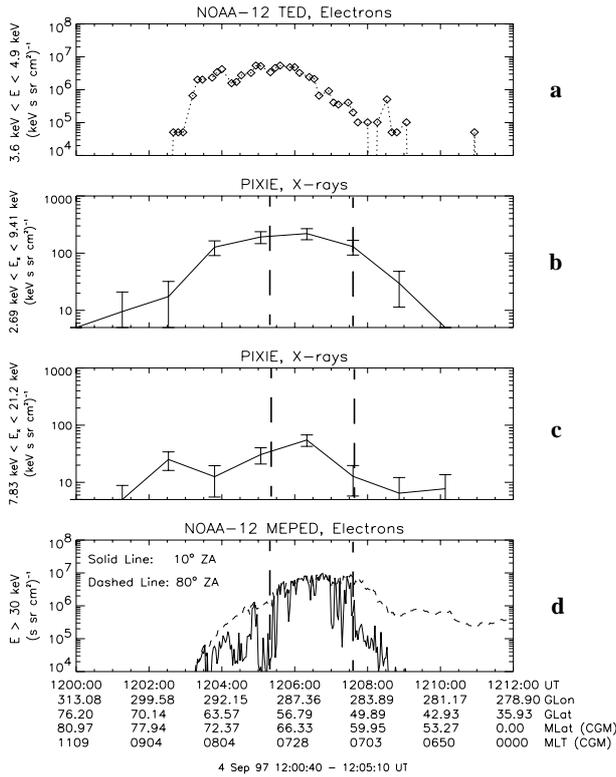
Figure 6. (a) Electron measurements within the loss cone from NOAA-12 (3.6-4.9 keV). (b) X-ray fluxes (2.7-9.4 keV) from PIXIE along the magnetic footprint of NOAA-12 satellite accumulated from 1200 to 1205 UT. (c) X-ray fluxes (7.8-21.2 keV) from PIXIE along the trajectory of NOAA-12 satellite, accumulated from 1202 to 1210 UT. (d) Electron measurements (>30 keV) at 10˚ (solid line) and 80˚ (dashed line) local zenith angle from NOAA-12. (e) PIXIE image (2.7-9.4 keV) accumulated from 1200:40 to 1205:00 UT showing the trajectory of the NOAA-12 satellite. The grid is corrected geomagnetic coordinates. The dashed vertical lines through panel 2-4 indicate the boundary of isotropic electron flux >30 keV.

Figure 7. (a) Electron measurements within the loss cone from DMSP-F13 (>4.9 keV). (b) X-ray fluxes (2.7-9.4 keV) from PIX-IE along the magnetic footprint of DMSP F13 satellite accumulated from 1215:40 to 1220:00 UT. (c) X-ray fluxes (7.8-21.2 keV) from PIXIE along the trajectory of DMSP F13 satellite accumulated from 1220 to 1228 UT. (d) Electron measurements (>20.8 keV) within the loss cone from DMSP-F13. (e) PIXIE image (2.7-9.4 keV) accumulated from 1215:40 to 1220:00 UT showing the trajectory of the DMSP-F13 satellite. The grid is corrected geomagnetic coordinates.

and Atmospheric Administration spacecraft 12 (NOAA-12) and Defense Meteorological Satellite Program spacecraft F13 (DMSP F13) are both in a near circular polar orbit at about 800 km altitude. The measurements from NOAA-12 (Figure 6) are compared with measured X rays along the magnetic footprint of the satellite averaged within a circle with a diameter of about 500 km The spatial resolution of the PIXIE images from these apogee passes is 1000 km. However, as long as the averaging area is significantly
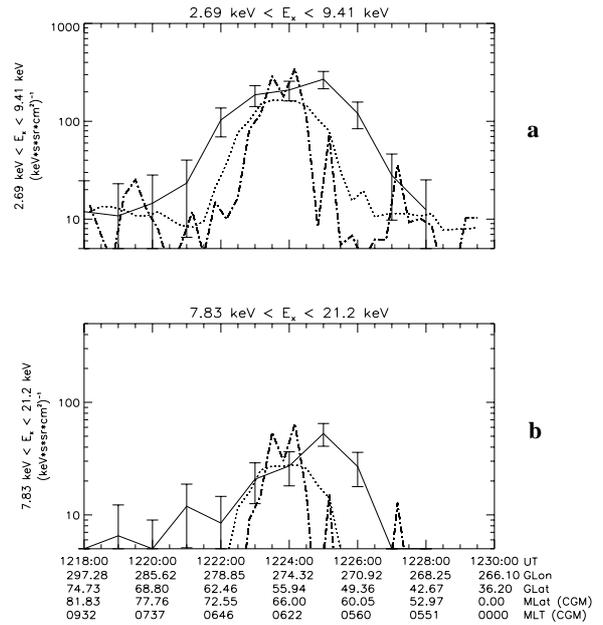
smaller than the spatial resolution of the pinhole camera itself, the resulting spatial resolution of the X-ray profiles is basically determined by the spatial resolution of the camera, i.e., 1000 km. Figure 6a shows the electron fluxes from one of the channels of the Total Energy Detector (TED) [Raben et al., 1995] looking at 10˚ local zenith angle, which corresponds to pitch angles <25˚ at these latitudes. The low-energy X-ray emission in Figure 6b is accumulated from 1200:40 to 1205:00 UT, due to the restriction given by the duty cycling of the front chamber of the PIXIE
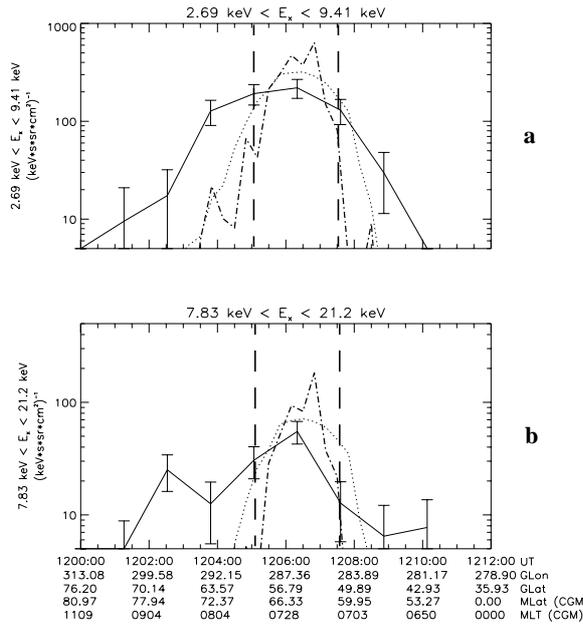
Figure 8. Measured and calculated X-ray fluxes along the magnetic footprint of the NOAA-12 satellite for September 4, 1997. Solid lines show the measured X-ray fluxes. Dotted lines show the calculated X-ray production from the electron spectra measured by TED and MEPED onboard NOAA-12. Dashed dotted lines show the unsmoothed calculated X-ray flux. (a) X-ray fluxes in the energy range from 2.7 to 9.4 keV, accumulated from 1200 to 1205 UT. (b) X-ray fluxes in the energy range from 7.8 to 21.2 keV, accumulated from 1202 to 1210 UT. The dashed vertical lines through panel 2-4 indicate the boundary of isotropic electron flux >30 keV (see Figure 6).

Figure 9. Measured and calculated X-ray fluxes along the magnetic footprint of the DMSP F13 satellite for September 4, 1997. Solid lines show the measured X-ray fluxes. Dotted lines show the smoothed calculated X-ray production from the electron spectra measured by SSJ/4 particle detector onboard DMSP F13. Dashed dotted lines show the unsmoothed calculated X-ray flux. (a) X-ray fluxes in the energy range from 2.7 to 9.4 keV, accumulated from 1215 to 1220 UT. (b) X-ray fluxes in the energy range from 7.8 to 21.2 keV, accumulated from 1220 to 1228 UT.

instrument. As the rear chamber is continuously operating the high-energy range X rays in Figure 6c are accumulated from 1202 to 1210 UT to be consistent with the electron measurements. Figure 6d shows the integral electron flux >30 keV measured by the Medium Energy Proton and Electron Detector (MEPED) [Raben et al., 1995] looking at 10° local zenith angle (solid line) and 80° local zenith angle (dashed line). During the pass these zenith angles correspond to 0°-25° and 65°-95° pitch angle intervals, which give us information about the boundaries of isotropic precipitation of electrons >30 keV. These boundaries are marked with dashed vertical lines in Figure 6. NOAA-12 is passing the X-ray source area from 1202 to 1210 UT, which means that the measurements of the lower X-ray energies (Figure 6b) are not consistent in time after 1205 UT. However the comparison indicates that the morning precipitation seems to be quite stable. In Figure 7 the electron measurements from the SSJ/4 [Hardy et al., 1984] detector onboard DMSP-F13 looking at local zenith, which corresponds to pitch angles <15° at these latitudes, are compared with the X-ray emission accumulated from 1215:40 to 1220:00 UT along the magnetic footprint of the satellite for the lower X-ray energies but from 1220 to 1228 UT for the high-energy X rays. DMSP-F13 is passing the area from 1220 to 1228 UT, which means that the measurements are not consistent in time for the lower X-ray energies. But again the comparison indicates that the morning precipitation seems to be quite stable.

In Figure 8 we show the measured X-ray fluxes along the magnetic footprint of the NOAA-12 satellite together with the calculated production of X rays from the electron spectra measured by the NOAA-12 loss cone detectors from 1200 to 1212 UT. In Figure 8a the production of X rays in the low-energy range are shown compared to the measured X rays accumulated from 1200 to 1205 UT and in Figure 8b the production of the high-energy range X rays are compared with the measured X rays accumulated from 1202 to 1210 UT. To obtain the X-ray production we use the 20 s integrated electron spectra and make a sum of two exponentials fit to each spectrum along the trajectory. The choice of a two exponentials fit to the electron spectra enables us to include the broad knee in the electron spectra around ~10-20 keV which is frequently observed in the morning sector [Østgaard et al., 1998, Sharber et al., 1998]. The energy spectra from NOAA-12 are obtained from the TED detector giving counts in four energy channels in the energy interval 0.3-4.9 keV and the MEPED detector giving integral counts >30 keV, >100 keV and >300 keV at pitch angles <25°. A look-up table assuming isotropic electron precipitation gives us the X-ray production emitted at different zenith angles as a function of single exponentials. This look-up table is provided by a coupled electron photon transport code originally derived from neutron transport codes [Lorence, 1992]. In this case the transport is of electrons and photons, and includes bremsstrahlung production, Compton scattering, photo-absorption, and radiation by secondary electrons. By adding the X-ray outcome from the two exponentials and integrating the X-ray fluxes in the energy ranges 2.7-9.4 keV and 7.8-21.2 keV we get the calculated X rays from each electron spectrum. The profiles of

the calculated X-ray production are smoothed by a running average of 140 seconds (i.e., over 1000 km along the satellite orbit) in order to be comparable to the spatial resolution of the measured X-ray profiles, which is about 1000 km. As can be seen from Figure 8 the calculated X rays from the electron spectra are in fairly good agreement with the directly measured X rays in both energy ranges of X rays within the boundary of isotropic electron precipitation (dashed vertical lines). The discrepancy is within the statistical errors of the measurements in this region. In the regions of anisotropic electron precipitation the calculation gives us too small X-ray fluxes. As our look-up tables are based on the assumption of isotropic electron fluxes the discrepancy in the anisotropic region are most probably due to X rays produced by the higher electron fluxes at pitch angles >25°. In Figure 6d the presence of anisotropic fluxes with large electron fluxes at pitch angles >65° is clearly seen. Assuming the X-ray production to be at 100 km altitude the loss cone at 800 km is within pitch angles of ~50°. As our spectra are obtained at pitch angles <25° the X-ray production are probably under-estimated in the region of anisotropic electron precipitation. Another source of discrepancy is introduced if the electron precipitation is structured. Such structures would be smoothed by the PIXIE FOV, but not by the point measurements of particles.

In Figure 9 we show the measured X-ray fluxes along the magnetic footprint of the DMSP F13 satellite together with the calculated production of X rays from the electron spectra measured by DMSP F13 from 1218 to 1230 UT. In Figure 9a the production of X rays in the low-energy range is shown compared to the measured X rays accumulated from 1215 to 1220 UT (time interval is restricted by the duty cycling of the front chamber of PIXIE). In Figure 9b panel the production of the high-energy range X rays is compared with the measured X rays accumulated from 1220 to 1228 UT. To obtain the X-ray production we use the 20 s integrated electron spectra and make a sum of two exponentials fit to each spectrum along the trajectory. The energy spectra from DMSP F13 are obtained from the SSJ/4 particle detector giving counts in 19 energy channels logarithmically spaced from 30 eV to 30 keV at pitch angles <15°. We have used the same procedure and the same look-up tables of X-ray production as for the NOAA-12 electron spectra. The profile of X-ray production is shown as dashed dotted lines. A smoothed profile (running average of 140 seconds, i.e., 1000 km to be consistently compared with the measured X-ray profiles) is plotted by dotted lines. As can be seen from Figure 9a the peak of the smoothed profile is close the measured X rays in the low energy range when the statistical uncertainties are taken into account. The DMSP F13 measurements give no spectral information of the electrons above 30 keV, but in the region of poor correlation the fluxes in the high-energy range electrons (within 15° pitch angle) falls off rapidly (not shown) and are so low that fluxes above 30 keV probably can not account for the discrepancy between measured and calculated X rays. From DMSP F13 we have no information about the electron precipitation at pitch angles >15°, but based on our findings from the NOAA-12 pass we interpret the region of good agreement to be the region of high electron fluxes i.e., the isotropic precipitation region. North and south of this region we calculate too low X-ray fluxes. The most probable explanation for this discrepancy is that our assumption of isotropic electron fluxes fails in this region and that the observed X rays are produced by larger electron fluxes at pitch angles >15°. Another source of discrepancy is again the probability of structured features in the electron precipitation. For the high energy range, Figure 9b, the peak of smoothed

calculated X rays is close to the measured X rays. The adjacent measured points are close to the calculated profile when statistical uncertainties are taken into account. At about 60° CGM latitude the measured X rays exceed the calculated X rays, which may be due to X rays produced by the anisotropic electron distribution in this area.

3. Conclusions

By examining an isolated substorm from September 4, 1997 we have found many of the same characteristics as reported in the statistical study of Østgaard et al. [1999b].

1. Growth phase signatures of directly driven precipitation at in the postnoon and dusk sector are not seen by PIXIE but clearly seen in the UV substorm, indicating mainly soft precipitation.

2. The substorm onset is seen simultaneously by UVI and PIXIE and correlates fairly well with the dipolarization and injection signatures seen in the magnetotail at 10 R_E.

3. During the expansion phase the X-ray emission source region is expanding dawnward.

4. During the recovery phase a localized maximum of X-ray emission is seen in the morning sector.

5. The delay times between the onset of the localized maximum of X rays in the morning sector relative to the substorm onset time in the midnight sector, are found to be consistent with drifting electrons in the energy range of 90-170 keV for 8 isolated substorms from 1996 and 1997. This strongly indicates that the maximum of precipitation observed in the morning sector is not caused by any new source region in the morning sector of the magnetosphere but rather by electrons injected close to midnight, drifting into the morning sector due to their gradient and curvature drift in the inhomogeneous magnetic field.

By examining the electron measurements from two passes of low-altitude satellites through the localized maximum of X-ray emission seen in the morning sector we may also conclude:

6. The X-ray fluxes calculated from the electron precipitation measured by the satellites in the morning sector are in fairly good agreement with the directly measured X rays by PIXIE in the region of isotropic electron precipitation.

7. Our method for calculating the X-ray fluxes are based on the assumption of isotropic electron precipitation and the input for our calculations are the electron spectra measured at small pitch angles. In the regions of anisotropic electron precipitation these spectra can not represent the entire loss-cone electron distribution. The observed X-ray fluxes are probably produced by higher fluxes of electrons at larger pitch angles but still within the loss-cone. The lack of high-energy electron measurements and the presence of structured features of precipitation will introduce additional uncertainties.

References

Akasofu, S.-I., 1964. The development of the auroral substorm, Planetary and Space Science, 12, 273–282.

Akasofu, S.-I., 1968. Polar and Magnetospheric Substorms, D. Reidel, Norwell, Mass.

Berkey, F. T., Driatskij, V. M., Henriksen, K., Hultqvist, B., Jelly, D., Shchuka, T. I., Theander, A., Yliniemi, J., 1974. A synoptic investigation of particle precipitation dynamics for 60 substorms in IQSY(1964-65) and IASY(1969), Planetary and Space Science, 22, 255–307.

Bjordal, J., Trefall, H., Ullaland, S., Bewersdorff, A., Kangas, J., Tanskanen, P., Kremser, G., Saeger, K. H., Specht, H., 1971. On the morphology of auroral-zone X-ray events, I, Dynamics of midnight events, Journal of Atmospheric and Terrestrial Physics, 33, 605–626.

Chenette, D. C., Datlowe, D. W., Imhof, W. L., Schumaker, T. L., Tobin, J. D., 1992. Global spectroscopy and imaging of atmospheric X-ray bremsstrahlung: Instrumentation and initial results from the PEM/ AXIS instrument aboard the Upper Atmosphere Research Satellite, SPIE Proceedings: Intstrumentation for Planetary and Terrestrial Atmosphere Remote Sensing., edited by Chakrabarti, S., Christensen, A. B., vol. 1745, 16–25.

Feldstein, Y. I., Starkov, G. V., 1967. Dynamics of auroral belt and polar geomagnetic disturbances, Planetary and Space Science, 15, 209.

Hardy, D. A., Gussenhoven, M. S., Holeman, E., 1985. A statistical model of auroral electron precipitation, Journal of Geophysical Research, 90, 4229–4248.

Hardy, D. A., Schmitt, L. K., Gussenhoven, M. S., Marshall, F. J., Yeh, H. C., Shumaker, T. L., Hube, A., Pantazis, J., 1984, Precipitating electron and ion detectors (SSJ/4) for the block 5D/flights 6-10 DMSP satellites: Calibartion and data presentation. Report AFGL-TR-84-0317, Air Force Geophysical Laboratory, Hanscom Air Force Base, Mass.

Hartz, T. H., Brice, N. M., 1967. The general pattern of auroral particle precipitation, Planetary and Space Science, 15, 301–329.

Imhof, W. L., Kilner, J. R., Nakano, G. H., Reagan, J. B., 1980. Satellite X-ray mappings of sporadic auroral zone electron precipitation events in the local dusk sector, Journal of Geophysical Research, 85, 3347–3359.

Imhof, W. L., Spear, K. A., Hamilton, J. W., Higgings, B. R., Murphy, M. J., Pronko, J. G., Vondrak, R. R., McKenzie, D. L., Rice, C. J., Gorney, D. J., Roux, D. A., Williams, R. L., Stein, J., Bjordal, J., Stadsnes, J., Njøten K., Rosenberg, T. J., Lutz, L., Detrick, D., 1995. The Polar Ionospheric X-ray Imaging Experiment (PIXIE), Space Science Review, 71, 385–408.

Isenberg, P. A., Koons, H. C., Fennell, J. F., 1982. Simultaneous observations of energetic electrons and dawnside chorus in geosynchronous orbit, Journal of Geophysical Research, 87, 1495–1503.

Jelly, D., Brice, N., 1967. Changes in Van Allen radiation associated with polar substorms, Journal of Geophysical Research, 72, 5919–5931.

Jentsch, V., 1976. Electron precipitation in the morning sector of the auroral zone, Journal of Geophysical Research, 81, 135–146.

Kangas, J., Lukkari, L., Tanskanen, P., Trefall, H., Stadsnes, J., Kremser, G., Riedler, W., 1975. On the morphology of auroral-zone X-ray events, IV, Substorm-related electron precipitation in the local morning sector, Journal of Atmospheric and Terrestrial Physics, 37, 1289–1303.

Lew, J. A., 1961. Drift rate in a dipole field, Journal of Geophysical Research, 66, 2681–2685.

Liou, K., Newell, P. T., Meng, C. I., 1997. Synoptic auroral distribution: A survey using polar ultraviolet imagery, Journal of Geophysical Research, 102, 27,197–27,205.

Lorence, L. J., 1992. CEPXS/ONELD Version 2.0: A discrete ordinates code package for general one-dimensional coupled electron-photon transport, IEEE Transactions on Nuclear Science, 39, 1031–1034.

McDiarmid, I. B., Burrows, J. R., Budzinski, E. E., 1975. Average characteristics of magnetospheric electrons (140 eV to 200 keV) at 1400 kilometers, Journal of Geophysical Research, 80, 73–79.

Østgaard, N., Stadsnes, J., Aarsnes, K., Søraas, F., Måseide, K., Smith, M., Sharber, J., 1998. Simultaneous measurements of X rays and electrons during a pulsating aurora, Annales Geophysicae, 16, 148–160.

Østgaard, N., Bjordal, J., Stadsnes, J., Thorsen, E.,1999a, PIXIE data processing at the University of Bergen. Report 1999-05, ISSN 0803-2696, University of Bergen.

Østgaard, N., Stadsnes, J., Bjordal, J., Vondrak, R. R., Cummer, S. A., D. Chenette, Parks, G. K., Brittnacher, M. J., McKenzie, D. L., 1999b. Global scale electron precipitation features seen in UV and X rays during substorms, Journal of Geophysical Research, 104, 10,191–10,204.

Parrot, M., Gaye, C. A., 1994. A statistical survey of ELF waves in a geostationary orbit, Geophysical Research Letters, 21, 2463–2466.

Petrinec, S. M., Mobilia, J., Chenette, D., Imhof, W. L., Fenrich, F., 1998. Statistical survey of auroral X-ray emissions: PIXIE observations, in Proceedings of the International Conference on Substorms, vol. 4, edited by Y. Kamide, pp. 809–812, Terra Science, Tokyo.

Raben, V. J., Evans, D. S., Sauer, H. H., Sahm, S. R., and Huynh, M., 1995. TIROS/NOAA satellite environment monitor data archive documentation: 1995 update, Technical Report, Space Environment Laboraty, Boulder, Colorado, USA.

Robinson, R. M., Vondrak, R. R., 1994. Validation of techniques for space based remote sensing of auroral precipitation and its ionospheric effect., Space Science Review, 69, 331–407.

Roederer, J. G., 1970. Dynamics of Geomagnetically Trapped Radiation, Springer Verlag, New York.

Sharber, J. R., Frahm, R. A., Link, R., Crowly, G., Winningham, J. D., E. E. Gaines, Nightingale, R. W., Chenette, D. L., Anderson, B. J., Gurgiolo, C. A., 1998. UARS Particle Enviroment Monitor observations during the november 1993 storm: Auroral morphology, spectral characterization, and energy deposition, Journal of Geophysical Research, 103, 26,307–26,322.

Sletten, A., Stadsnes, J., . Trefall, H., 1971. Auroral-zone X-ray events and their relation to polar magnetic substorms, Journal of Atmospheric and Terrestrial Physics, 33, 589–604.

Torr, M. R., Torr, D. G., Zukic, M., Johnson, R. B., Ajello, J., Banks, P., Clark, K., Cole, K., Keffer, C., Parks, G., Tsurutsani, B., Spann, J., 1995. A far ultraviolet imager for the international solar-terrestrial physics mission., Space Science Review, 71, 329–383.